Near-Earth thin current sheets and Birkeland currents during substorm growth phase

Sorin Zaharia[1] and C. Z. Cheng

Plasma Physics Laboratory, Princeton University, Princeton, New Jersey, USA

Received 1 April 2003; revised 5 July 2003; accepted 23 July 2003; published 4 September 2003.

[1] Two important observed substorm growth phase phenomena are modeled: the formation of a near-Earth ($|X| \sim 8\ R_E$) thin cross-tail current sheet, as well as the equatorward shift of the ionospheric Birkeland currents. Our study is performed by solving the 3D force-balance equation with realistic boundary conditions and pressure distributions. The obtained cross-tail current sheet has large current density ($J_\phi \sim 10$ nA/m^2) and a half-thickness in the north-south direction of $\sim$1 R_E, while plasma β is very high ($\beta \sim 40$) in the current sheet region. The Region-1 and Region-2 Birkeland currents, formed on closed field lines due to pressure gradients, move equatorward and become more intense ($J_{\|\max} \sim 3$ μA/m^2) compared to quiet times. The results agree with growth phase observations. We also find that the cross-tail current sheet maps into the ionosphere in the transition region between the Region-1 and Region-2 currents. *INDEX TERMS:* 2740 Magnetospheric Physics: Magnetospheric configuration and dynamics; 2708 Magnetospheric Physics: Current systems; 2730 Magnetospheric Physics: Magnetosphere—inner; 2788 Magnetospheric Physics: Storms and substorms. **Citation:** Zaharia, S., and C. Z. Cheng, Near-Earth thin current sheets and Birkeland currents during substorm growth phase, *Geophys. Res. Lett.*, *30*(17), 1883, doi:10.1029/2003GL017456, 2003.

1. Introduction

[2] Two important phenomena are observed during the substorm growth phase. One is the appearance of a thin cross-tail current sheet in the near-Earth (7–10 R_E) plasma sheet [e.g., *Sergeev et al.*, 1990]. The other consists in an intensity increase and equatorward shift of the Region-1 and Region-2 (from here on, R-1 and R-2) ionospheric field-aligned (Birkeland) currents. Using our 3D quasi-static equilibrium model [*Cheng*, 1995; *Zaharia et al.*, 2003] we investigate the cross-tail current sheet formation and the Birkeland currents, as well as their relationship during the substorm growth phase.

[3] There is a consensus in the space physics community that the inner/middle magnetosphere on closed field lines is a "slow-flow" region [*Wolf*, 1983] at most times, including during the substorm growth phase. Thus inertial terms can be neglected in the plasma momentum equation and the system evolution can be depicted as a temporal series of "snapshots", each of them a "quasi-static" equilibrium in which force balance is maintained between the Lorentz and plasma pressure gradient forces. Within the "slow-flow" approximation several studies have tried to explain thin current sheet formation. Some [e.g., *Birn and Schindler*, 2002] investigate the distant-tail currents at $X < -20\ R_E$ (X, Y and Z are the GSM coordinates), where the "tail approximation" [*Birn et al.*, 1975] is valid. Only a few studies [e.g., *Becker et al.*, 2001] analyze the currents closer to Earth, where the tail approximation becomes inaccurate, and these studies assume 2-D axisymmetry, missing the Birkeland current formation, a 3D effect [*Cheng*, 1995]. Most studies consider the magnetospheric evolution during the growth phase to be dictated by "adiabatic convection" [e.g., *Wolf*, 1983] whereby the entropy, related to $S = PV^\gamma$, is conserved (P is the pressure, V the magnetic flux tube volume per unit flux, $V = \int ds/B$, with the integral performed along the magnetic field line; $\gamma = 5/3$). With entropy conservation constraints a very thin current sheet can form due to magnetopause boundary deformations [*Birn and Schindler*, 2002].

[4] In the inner tail ($|X| < 15\ R_E$) there are observational indications however [e.g., *Borovsky et al.*, 1998] that entropy conservation is violated. A process called entropy anti-diffusion has been proposed [*Lee et al.*, 1998] to explain thin current sheet formation in such a situation. The magnetospheric evolution in the model of *Lee et al.* [1998] is however characterized by significant flows, a result not supported by growth phase observations.

[5] In this letter we discuss 3D force-balanced magnetospheric states, focusing on the formation during the substorm growth phase of a thin current sheet in the near-Earth plasma sheet and on the changes in Birkeland currents compared to quiet times. Our configurations are obtained by numerically solving the force-balance equation $\mathbf{J} \times \mathbf{B} = \nabla P$ [*Cheng*, 1995; *Zaharia et al.*, 2003], with $\mathbf{B}$ expressed by Euler potentials as $\mathbf{B} = \nabla\psi \times \nabla\alpha$ (ψ is the magnetic flux, and α an azimuthal angle-like variable) and using realistic boundary conditions and pressure distributions. The obtained current sheet is localized at $-10\ R_E < X < -7\ R_E$, $-6\ R_E < Y < 6\ R_E$, has a maximum density $\sim$11 nA/m^2 and a half-thickness of $\sim$1 R_E. The cause of its formation is the large $|\partial P/\partial\psi|$ caused by plasma and flux transport [e.g., *Erickson*, 1992] during the growth phase. The Birkeland currents, formed on closed field lines due to pressure gradients, move equatorward and become more intense ($J_{\|\max} \sim 3$ μA/m^2) compared to quiet times. The cross-tail current sheet region maps into the ionosphere in the transition region between the R-1 and R-2 currents.

2. Modeling Approach

[6] We work in a flux coordinate system $\{\psi, \alpha, \chi\}$, with α and ψ being the Euler potentials introduced above. The third coordinate, χ, is a function of the distance along the field line. The computation of equilibria in the $\{\psi, \alpha, \chi\}$ system,

[1]Now at Los Alamos National Laboratory.

Copyright 2003 by the American Geophysical Union.
0094-8276/03/2003GL017456$05.00

described in detail elsewhere [*Cheng*, 1995; *Zaharia et al.*, 2003], consists in solving the 3D equation $\mathbf{J} \times \mathbf{B} = \nabla P$ iteratively, subject to input pressure distribution and boundary conditions. The boundary ψ surfaces delimiting the computational domain have specified shapes, obtained [*Zaharia et al.*, 2003] from empirical models such as T96 [*Tsyganenko and Stern*, 1996]. We only briefly describe here the changes implemented in our method for a more accurate computation of configurations with strong current sheets. The first change was using as "planet boundary" a sphere of radius 2 R_E instead of the Earth's surface. While the code can handle a computation from 1 R_E, this was done to save grid points for the important plasma sheet region. The second change was relaxing the "equal arc length" choice [*Cheng*, 1995] for χ, instead concentrating the grid points in the plasma sheet. The points are also non-uniformly distributed in azimuth [*Zaharia et al.*, 2003], with a concentration near the midnight meridian. We use $N_\psi \times N_\alpha \times N_\chi = 75^3$ grid points, leading to a spatial resolution near the equatorial plane at $R \sim 8\ R_E$ and midnight of about $\Delta X = 0.25\ R_E$, $\Delta Y = 0.25\ R_E$ and $\Delta Z = 0.05\ R_E$.

3. Results: Quiet Time vs. Growth Phase

[7] While our emphasis is on the substorm growth phase, we will present first a 3D force-balanced quiet-time configuration, in order to allow a discussion of differences between the two. For the quiet time we use inner and outer boundary shapes for ψ obtained by field-line tracing using the T96 model, with parameters $DST = -5$ nT, $P_{SW} = 2.1$ nPa, $B_{yIMF} = 0$ and $B_{zIMF} = 1$ nT, representing average quiet-time values as obtained from the OMNI solar wind database. For the pressure P we choose the following form in the equatorial plane:

$$P(R, \phi, Z = 0) = 89e^{-0.59R}\left[A + Be^{-\left(\frac{\phi-\pi}{\Delta\phi}\right)^2}\right] + 8.9R^{-1.53} \cdot \left[C + De^{-\left(\frac{\phi-\pi}{\Delta\phi}\right)^2}\right] \quad (1)$$

where R, ϕ, Z define the usual cylindrical coordinate system with Earth as origin and $\phi = \pi$ at midnight, while A, B, C, D and $\Delta\phi$ are constants. We choose $A = B = 0.5$, $C = 2$, $D = -1$ and $\Delta\phi = 0.5\pi$, such that for $\phi = \pi$ equation (3) recovers the Spence-Kivelson empirical formula [*Spence and Kivelson*, 1993] which is based on observations at midnight. Also, since the first term on the RHS of equation (3) dominates close to Earth ($R < 10\ R_E$), while the second farther in the tail, equation (3) also simulates for a given R an azimuthal maximum in P at midnight close to Earth, and an azimuthal minimum farther in the tail. This qualitative local-time dependence, seen in the equatorial P contours in Figure 1b, is justified by observations showing a maximum in P at midnight close to Earth [e.g., *De Michelis et al.*, 1999], but a slight minimum at midnight for $R > 10\ R_E$ (see Figure 11 of [*Tsyganenko and Mukai*, 2003]). We assume an east-west symmetry in the P distribution, a result found from averaged GEOTAIL plasma sheet observations [*Tsyganenko and Mukai*, 2003] beyond 10 R_E. We note that other observations [*Wing and Newell*, 1998] and convection simulations [*Wang et al.*, 2003] do find an east-west asymmetry even beyond 10 R_E.

[8] We will only briefly describe the computed quiet-time state. The cross-tail current density ($J_\phi = \mathbf{J} \cdot \nabla\phi/|\nabla\phi|$) has a

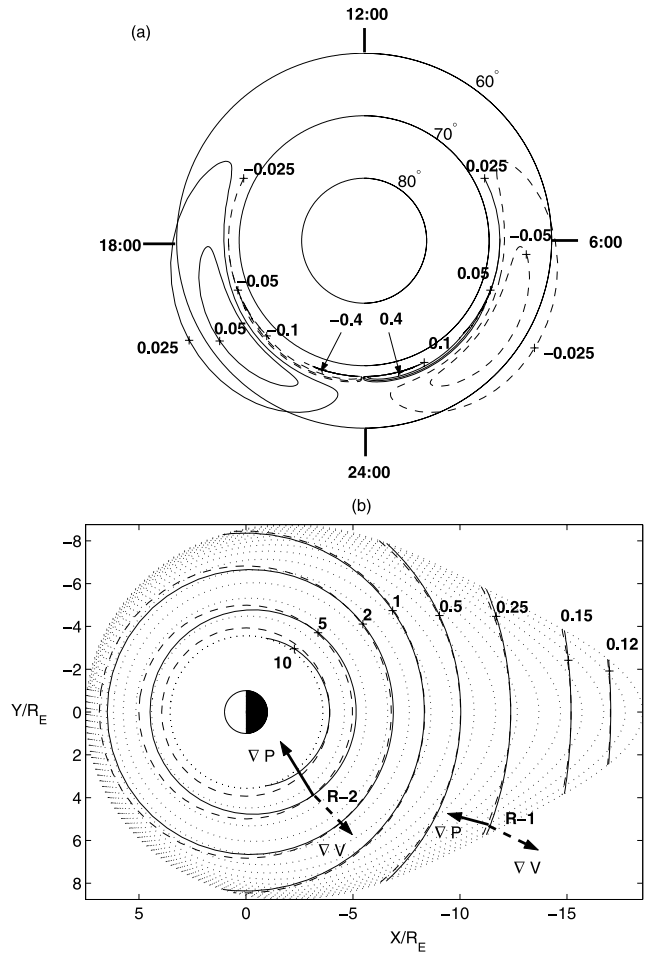

Figure 1. For the quiet-time state: (a) Contours of constant ionospheric $J_\parallel$ (μA/m^2); solid (dashed) lines represent currents into (out of) the ionosphere; (b) Equatorial plane contours of P (nPa) (solid) and V (dashed); also shown are ∇P and ∇V at two points mapping into regions of opposite $J_\parallel$ in the ionosphere; the dotted lines show const. ψ contours.

maximum of 2.4 nA/m^2. Dashed lines in Figure 2a show Sun-Earth axis profiles of P, B and plasma β for this case, while the Birkeland currents are shown in Figure 1a. The R-2 currents span a broad area, but are very weak ($J_{\parallel 2\max} = 0.07\ \mu$A/m^2) — consistent with observations [*Iijima and Potempra*, 1976] showing their virtual disappearance during quiet times. A more narrow R-1 current pattern exists at higher latitudes ($\sim$68°), with maximum densities ($\approx$0.5 μA/m^2) at 22:30 and 1:30 magnetic local times (from here on MLT), again agreeing very well with quiet-time observations [*Iijima and Potempra*, 1976]. The R-1 and R-2 current formation mechanism is easily understood from Vasyliunas relation [*Vasyliunas*, 1970]:

$$\left.\frac{J_\parallel}{B}\right|_{iono} = \frac{\mathbf{B}_{eq}}{B_{eq}^2} \cdot \left(\nabla V \times \nabla P_{eq}\right) \quad (2)$$

[9] The quantity $\mathbf{B}_{eq} \cdot (\nabla P_{eq} \times \nabla V)$ has opposite signs for R-1 vs. R-2 current formation, as seen in Figure 1b, which shows ∇P and ∇V at two equatorial plane locations that map into the ionosphere in regions of opposite $\mathbf{J}_\parallel$.

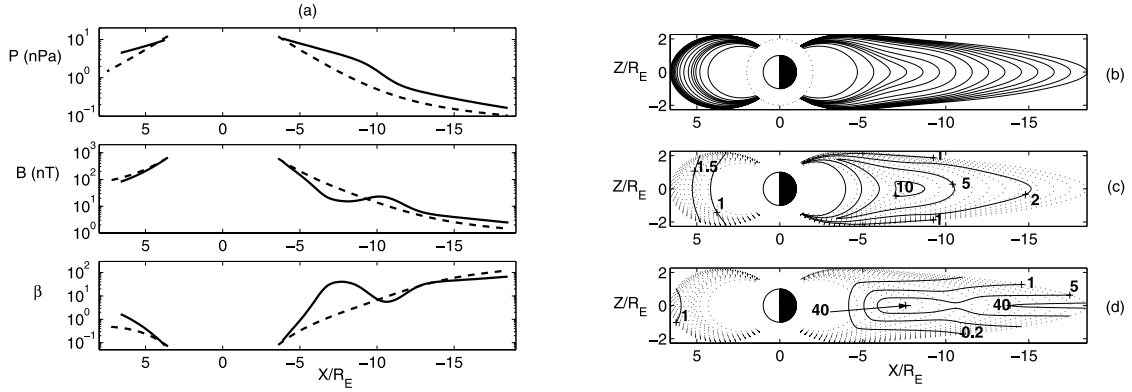

Figure 2. (a) Profiles of P, B and β along the Sun-Earth axis for the growth phase (solid) and quiet time (dashed); For the growth phase, plots in the noon-midnight meridian plane of: (b) Magnetic field lines; (c) Constant J_ϕ (solid) and ψ (dotted) contours; (d) Constant β (solid) and ψ (dotted) contours.

[10] For modeling a substorm growth phase, the ψ boundary shapes are again obtained from T96, but with P_{SW} = 5 nPa, $B_{ZIMF} = -5$ nT, B_{YIMF} = 0.5 nT and $DST = -50$ nT, typical for active times. There are only scarce pressure observations during the growth phase. While P increases with activity throughout the plasma sheet [e.g., *Tsyganenko and Mukai*, 2003], observations [e.g. *Spence et al.*, 1989] as well as convection simulations [*Wang et al.*, 2003] show that the enhancement is larger at smaller R. Another property, both observed [*Wing and Newell*, 1998; *Tsyganenko and Mukai*, 2003] and simulated [e.g., *Wang et al.*, 2003], is the Earthward expansion of regions with azimuthal minimum P at midnight (for fixed R). We choose P in the equatorial plane as

$$P(R,\phi,Z=0) = 12.5e^{-0.25R}\cdot\left[A + B\tanh\left(\frac{x_1 - R}{\Delta R}\right)e^{-\left(\frac{\phi-\pi}{\Delta\phi}\right)^2}\right] + 8.9R^{-1.53}\left[C + De^{-\left(\frac{\phi-\pi}{\Delta\phi}\right)^2}\right] \quad (3)$$

with $A = 1.25$, $B = 0.75$, $C = 3$, $D = -2$, $\Delta_\phi = 0.3\pi$, $x_1 = 10$ and $\Delta R = 1.25$. The resulting Sun-Earth axis P profile, shown by solid lines in Figure 2a, has about twice the quiet-time value for $R > 10\ R_E$, and is even more enhanced closer to Earth. The equatorial P contours, shown in Figure 3b, show the Earthward expansion of regions with P minimum (for a given R) at midnight, and at the same time the more pronounced azimuthal minima in P as compared to the quiet-time case.

[11] Figure 2 shows several quantities in the computed force-balanced state for the growth phase. The solid lines in Figure 2a show Sun-Earth axis profiles of P, B and β. One notices the appearance of a magnetic well, with $B_{min} \approx$ 15 nT, between $X = -7\ R_E$ and $X = -10\ R_E$. In the well, β peaks at $\beta \approx 45$ near $X = -8\ R_E$. The **B**-field is extremely tail-like in the near-Earth plasma sheet, as seen in Figure 2b. This suggests a thin current sheet, which can indeed be seen in Figure 2c, which shows noon-midnight plane contours of J_ϕ. The maximum J_ϕ is $J_{\phi max} \approx 11$ nA/m^2 at $X = -8\ R_E$, and the current sheet has a half-width of $\sim$1 R_E there. Finally, from Figure 2d one notices that β is very large in the vicinity of the equatorial plane.

[12] The computed Birkeland currents are shown in Figure 3a. Both the R-1 and R-2 currents have moved to lower latitudes compared to the quiet-time case shown in Figure 1a, and are much more intense (with the intense $J_\parallel$ regions quite peaked in latitude). The R-2 current has a maximum density of 1.2 μA/m^2 at 22:00 and 2:00 MLT, and stretches between 60° and 62° latitude. The R-1 current is

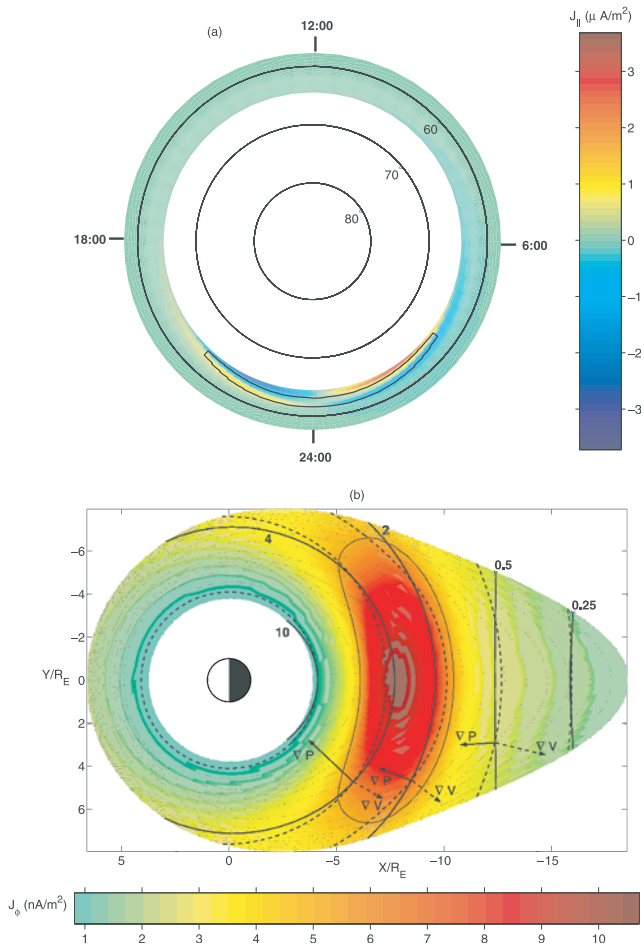

Figure 3. For the growth phase: (a) Ionospheric $J_\parallel$; (b) Equatorial plane P (nPa) contours (thick solid lines), V (dashed) and ψ (dotted), over a color plot of J_ϕ; the thin solid contour shows the region inside which $J_\phi > 0.5\ J_{\phi max}$; also shown are ∇P and ∇V at three locations.

found between 62° and 65°, with a maximum of 3.5 μA/m^2 and closer to midnight (22:30 and 1:30 MLT). Again, the different signs of $\mathbf{B} \cdot (\nabla P \times \nabla V)$ in the R-2 and R-1 current regions, respectively, are seen in Figure 3b, which shows the orientation of ∇P and ∇V over a color plot of J_ϕ in the equatorial plane. From Figure 3 one sees that the cross-tail current sheet maps into the ionosphere into the transition area between R-1 and R-2 currents.

4. Discussion and Summary

[13] We have modeled the quasi-static equilibrium magnetosphere during the substorm growth phase, by solving the 3D force-balance equation with realistic pressure and flux boundaries. The results include a thin current sheet with $J_\phi \sim$ 10 nA/m^2 in the near-Earth plasma sheet between 7 and 9 R_E. A minimum in the **B**-field appears there, also found in simulations with enhanced magnetospheric convection [*Erickson*, 1992; *Wang et al.*, 2003]. While the minimum of [*Wang et al.*, 2003] is at 10 R_E, farther than ours, they do not take into account the inward motion of the inner edge of the plasma sheet during active times (therefore one would expect the actual minimum to be closer than 10 R_E).

[14] We find both Region-2 and Region-1 Birkeland currents on closed field lines. The formation of R-1 currents in 3D equilibria has been modeled before [*Birn*, 1989] in the distant tail ($X < -20$ R_E). In this study, they appear on closed lines (as also found by [*Yang et al.*, 1994] on the flanks) much closer to Earth, due to pressure values higher at dawn and dusk than at midnight. Our 3D growth phase configuration has both the R-1 and R-2 currents moving toward lower latitudes (60°–65°) and becoming more intense ($J_{\|1\max} \sim 3$ μA/m^2) compared to quiet times.

[15] The near-Earth cross-tail current sheet has a half-thickness $\sim$1 R_E, agreeing with observations [*Sanny et al.*, 1994] showing the sheet being wider than 1 R_E throughout the growth phase. This result differs from the popular belief that the sheet thickness is on the order of an ion gyro-radius ($\rho_i \leq 1000$ km). We note that the sheet does not need to become thinner than $\sim$1 R_E to lead to substorm onset; indeed, our obtained β ($\sim$45) is sufficiently large for a kinetic ballooning instability [*Cheng and Lui*, 1998] to be excited and lead to onset.

[16] Based on our study, the scenario for cross-tail current sheet formation near Earth (7 $R_E < |X| < 10$ R_E) is as follows: during the growth phase, the increased solar wind P_{SW} and magnetopause flux merging lead to enhanced tail stretching. At the same time, the pressure in the near-Earth plasma sheet increases due to enhanced convection, leading to larger pressure gradients. Due to the tail flux tube stretching, the difference $\Delta\psi$ between ψ_{out} (on the outer boundary at $R \approx 18.5$ R_E) and ψ_{in} (on the inner one at $R \approx$ 3.5 R_E) becomes smaller. The increase in $|\partial P/\partial R|$ coupled with the decrease in $\partial\psi/\partial R$ leads to very large $|\partial P/\partial\psi|$ and thus current densities (at midnight $\alpha = \phi$ and $J_\phi = \mathbf{J} \cdot \nabla\phi/|\nabla\phi| = R\partial P/\partial\psi$) localized in the near-Earth plasma sheet.

[17] **Acknowledgments.** This work was supported by NASA grant No. W-10062 and DoE contract No. DE-AC02-76-CH03073. S. Zaharia would like to thank Dr. Jay R. Johnson for helpful discussions.

References

Becker, U., et al., On the quasistatic development of thin current sheets in magnetotail-like magnetic fields, *J. Geophys. Res.*, *106*(A3), 3811, 2001.

Birn, J., Three-dimensional equilibria for the extended magnetotail and the generation of field aligned current sheets, *J. Geophys. Res.*, *94*, 252, 1989.

Birn, J., and K. Schindler, Thin current sheets in the magnetotail and the loss of equilibrium, *J. Geophys. Res.*, *107*(A7), 1117, doi:10.1029/2001JA000291, 2002.

Birn, J., et al., Open and closed magnetospheric tail configurations and their stability, *Astrophys. and Space Sci.*, *35*, 389, 1975.

Borovsky, J. E., et al., The transport of plasma sheet material from the distant tail to geosynchronous orbit, *J. Geophys. Res.*, *103*, 20,297, 1998.

Cheng, C. Z., Three-dimensional magnetospheric equilibrium with isotropic pressure, *Geophys. Res. Lett.*, *22*, 2401, 1995.

Cheng, C. Z., and A. T. Y. Lui, Kinetic ballooning instability for substorm onset and current disruption observed by AMPTE/CCE, *Geophys. Res. Lett.*, *25*(21), 4091, 1998.

De Michelis, P., et al., An average image of proton plasma pressure and of current systems in the equatorial plane derived from AMPTE/CCE-CHEM measurements, *J. Geophys. Res.*, *104*, 28,615, 1999.

Erickson, G. M., A quasi-static magnetospheric convection model in two-dimensions, *J. Geophys. Res.*, *97*, 6505, 1992.

Iijima, T., and T. A. Potemra, The amplitude distribution of field-aligned currents at northern high latitudes observed by Triad, *J. Geophys. Res.*, *81*, 2165, 1976.

Lee, L. C., et al., Entropy antidiffusion instability and formation of a thin current sheet during geomagnetic substorms, *J. Geophys. Res.*, *103*, 29,419, 1998.

Sanny, J., et al., Growth-phase thinning of the near-Earth current sheet during the CDAW 6 substorm, *J. Geophys. Res.*, *99*(A4), 5805, 1994.

Sergeev, V. A., et al., Current sheet thickness in the near-earth plasma sheet during substorm growth phase, *J. Geophys. Res.*, *95*, 3819, 1990.

Spence, H. E., and M. G. Kivelson, Contributions of the low-latitude boundary layer to the finite width magnetotail convection model, *J. Geophys. Res.*, *98*, 15,487, 1993.

Spence, H. E., et al., Magnetospheric plasma pressures in the midnight meridian: Observations from 2.5 to 35 R_E, *J. Geophys. Res.*, *94*, 5264, 1989.

Tsyganenko, N. A., and T. Mukai, Tail plasma sheet models derived from Geotail particle data, *J. Geophys. Res.*, *108*(A3), doi:10.1029/2002JA009707, 2003.

Tsyganenko, N. A., and D. P. Stern, Modeling the global magnetic field of the large-scale Birkeland current systems, *J. Geophys. Res.*, *101*, 27,187, 1996.

Vasyliunas, V. M., Mathematical models of magnetospheric convection and its coupling to the ionosphere, in *Particles and Fields in the Magnetosphere*, edited by B. M. McCormac and D. Reidel, Hingham, MA, 60–71, 1970.

Wang, C. P., et al., Modeling the inner plasma sheet protons and magnetic field under enhanced convection, *J. Geophys. Res.*, *108*(A2), 1074, doi:10.1029/2002JA009620, 2003.

Wing, S., and P. T. Newell, Central plasma sheet ion properties as inferred from ionospheric observations, *J. Geophys. Res.*, *103*, 6785, 1998.

Wolf, R. A., The quasi-static (slow-flow) region of the magnetosphere, in *Solar-Terrestrial Physics*, 303–368, D. Reidel, Hingham, MA, 1983.

Yang, Y. S., et al., Generation of region-1 current by magnetospheric pressure gradients, *J. Geophys. Res.*, *99*, 223, 1994.

Zaharia, S., et al., 3-D Force-balanced magnetospheric configurations, *Ann. Geophys.*, in press, 2003.

S. Zaharia and C. Z. Cheng, Princeton University, Plasma Physics Laboratory, P.O. Box 451, Princeton, NJ 08543, USA. (szaharia@pppl.gov; fcheng@pppl.gov)